LETTER

doi:10.1038/nature11709

Tet1 controls meiosis by regulating meiotic gene expression

Shinpei Yamaguchi[1,2,3]*, Kwonho Hong[1,2,3]*, Rui Liu[4]*, Li Shen[1,2,3], Azusa Inoue[1,2,3], Dinh Diep[4], Kun Zhang[4] & Yi Zhang[1,2,3,5]

Meiosis is a germ-cell-specific cell division process through which haploid gametes are produced for sexual reproduction[1]. Before the initiation of meiosis, mouse primordial germ cells undergo a series of epigenetic reprogramming steps[2,3], including the global erasure of DNA methylation at the 5-position of cytosine (5mC) in CpG-rich DNA[4,5]. Although several epigenetic regulators, such as Dnmt3l and the histone methyltransferases G9a and Prdm9, have been reported to be crucial for meiosis[6], little is known about how the expression of meiotic genes is regulated and how their expression contributes to normal meiosis. Using a loss-of-function approach in mice, here we show that the 5mC-specific dioxygenase Tet1 has an important role in regulating meiosis in mouse oocytes. Tet1 deficiency significantly reduces female germ-cell numbers and fertility. Univalent chromosomes and unresolved DNA double-strand breaks are also observed in Tet1-deficient oocytes. Tet1 deficiency does not greatly affect the genome-wide demethylation that takes place in primordial germ cells, but leads to defective DNA demethylation and decreased expression of a subset of meiotic genes. Our study thus establishes a function for Tet1 in meiosis and meiotic gene activation in female germ cells.

Mouse primordial germ cells (PGCs) first appear at embryonic day (E)7.25 on the base of the allantois, and then migrate through the hindgut to the genital ridge[3]. During migration and at the genital ridge, PGCs undergo a series of coordinated epigenetic reprogramming, including global erasure of DNA methylation[4,5]. Recent demonstration that proteins of the Tet family are involved in DNA demethylation prompted us to evaluate the role of Tet proteins in PGC reprogramming[7–10]. Reverse transcriptase quantitative PCR (RT–qPCR) analysis demonstrated that *Tet1* is preferentially expressed in PGCs, whereas *Tet2* is expressed in both PGCs and somatic cells, and *Tet3* is mainly expressed in somatic cells during PGC development (E9.5–13.5) (Supplementary Fig. 1). To explore a potential role of Tet1 in PGC reprogramming and/or germ-cell development, we generated Tet1 gene-trap mice (Supplementary Fig. 2a–d). Homozygous mutant mice ($Tet1^{Gt/Gt}$) were generated by crossing heterozygous mice. Southern blot analysis, genomic sequencing and allele-specific PCR confirmed a single site insertion of a tandem-repeated gene-trap cassette into the first intron of the *Tet1* gene (Supplementary Fig. 2a–d). β-galactosidase activity analysis showed that the transgene is almost exclusively expressed in PGCs (Supplementary Fig. 2e), which is consistent with the *Tet1* expression pattern (Supplementary Fig. 1), supporting a single locus insertion. Western blot analysis demonstrated that the insertion nullified the expression of the full-length Tet1 protein (Supplementary Fig. 3a). As expected, a fusion protein between the first exon of Tet1 (amino acids 1–621) and β-geo (β-galactosidase plus neomycin resistance gene 1,303 amino acids) was detected in $Tet1^{Gt/Gt}$ embryonic stem (ES) cells. Consistent with loss of Tet1, dot-blot and mass spectrometry analyses showed about a 45% reduction of 5-hydroxymethylcytosine (5hmC) levels in E9.5 $Tet1^{Gt/Gt}$ embryos (Supplementary Fig. 3b–d). RT–qPCR analysis demonstrated that the *Tet1* level in E11.5 PGCs from $Tet1^{Gt/Gt}$ mice is less than 5% that of wild-type PGCs (Supplementary Fig. 3e). Consistently, Tet1 protein was also not detectable in spreads of $Tet1^{Gt/Gt}$ PGCs (Supplementary Fig. 3f). Furthermore, immunostaining revealed a loss of the dotted 5hmC staining signal in germ cells of the E14.5 $Tet1^{Gt/Gt}$ genital ridge (Supplementary Fig. 3g). Collectively, these data indicate that Tet1 expression is effectively abolished and the 5hmC level was significantly reduced in $Tet1^{Gt/Gt}$ PGCs.

Analysis of early backcross generations (N_{1-2}) revealed they were embryonic lethal for homozygous *Tet1* mutants, whereas heterozygous mutant mice were born at normal Mendelian ratios (Supplementary Table 1). Although further backcross generations (N_{3-6}) relieved the

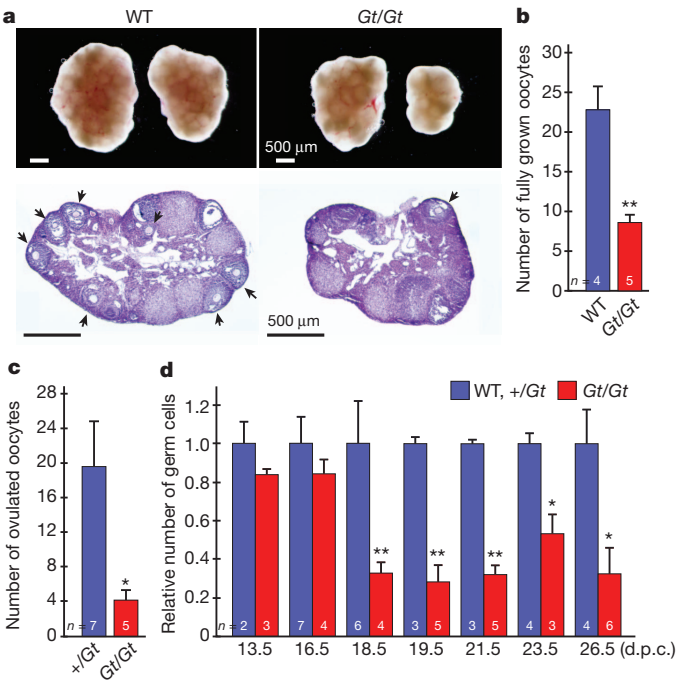

Figure 1 | The subfertility of $Tet1^{Gt/Gt}$ mice is associated with oocyte loss in the late embryonic stage. **a**, Abnormal ovaries of the $Tet1^{Gt/Gt}$ mice. Top, representative images of ovaries from 8-week-old wild-type (WT) and Tet1 mutant (*Gt/Gt*) mice. Both the left and right ovaries from one representative female are shown. Bottom, representative images of haematoxylin and eosin (H&E) staining of adult ovary sections. Arrows indicate fully grown oocytes. **b**, Number of fully grown oocytes in adult ovaries. $n = 4–5$. **c**, The average number of ovulated oocytes per female after hormonal stimulation. $n = 5–7$. Error bars indicate s.e.m. **d**, The relative oocyte numbers normalized to that in the control mouse. The number of oocytes in control mice was counted and set as 1. $n = 2–7$. d.p.c., days post coitum. All error bars indicate s.e.m. $*P < 0.05$; $**P < 0.01$.

[1]Howard Hughes Medical Institute, Harvard Medical School, WAB-149G, 200 Longwood Avenue, Boston, Massachusetts 02115, USA. [2]Program in Cellular and Molecular Medicine, Boston Children's Hospital, Harvard Medical School, WAB-149G, 200 Longwood Avenue, Boston, Massachusetts 02115, USA. [3]Department of Genetics, Harvard Medical School, WAB-149G, 200 Longwood Avenue, Boston, Massachusetts 02115, USA. [4]Departments of Bioengineering, University of California at San Diego, La Jolla, California 92093-0412 USA. [5]Harvard Stem Cell Institute, Harvard Medical School, WAB-149G, 200 Longwood Avenue, Boston, Massachusetts 02115, USA.
*These authors contributed equally to this work.

embryonic lethal phenotype, the number of viable homozygous mice is still only approximately one-third of the amount expected. Because the severity of embryonic lethality is affected by genetic background, we only used later than the N_6 generation of *Tet1*$^{Gt/Gt}$ mice for subsequent analyses. Similar to a recent report[11], reduced pup numbers were observed when either homozygous male or homozygous female animals were crossed with wild-type animals, and the pup numbers are even fewer when homozygous animals were crossed (Supplementary Fig. 4a). Because male gonad was morphologically normal and no obvious defects in male germ-cell development were observed (data not shown), our attention is focused on characterizing the female germ-cell phenotypes.

We found that the size of the *Tet1*$^{Gt/Gt}$ ovary is significantly smaller, with a 30% reduction in the ovary-to-body-weight ratio (Fig. 1a and Supplementary Fig. 4b). Interestingly, asymmetric ovary size caused by ovarian agenesis is frequently observed in the *Tet1*$^{Gt/Gt}$ animals (Fig. 1a). Both fully grown oocytes in the ovary and ovulated oocytes after hormonal stimulation are significantly reduced in the *Tet1*$^{Gt/Gt}$ animals (Fig. 1b, c). Ovary staining with germ-cell-specific markers (MVH, TRA98 and MSY2) followed by counting revealed a significant reduction in oocyte number from E16.5 to E18.5 (Fig. 1d and Supplementary Fig. 5a), concurrent with a significant increase in apoptotic oocytes (Supplementary Fig. 5b, c). These results suggest that increased apoptosis is probably one contributing factor for oocyte loss in *Tet1*$^{Gt/Gt}$ animals.

Because meiotic prophase takes place in the embryonic ovary, and meiotic defects can cause germ-cell apoptosis[12], we asked whether loss-of-function mutation of Tet1 might lead to a meiotic defect. Immunostaining of oocyte surface spreads with the meiotic marker SYCP3 and the centromere-marker CREST revealed that progression of meiotic prophase is severely impaired in *Tet1*$^{Gt/Gt}$ animals. About 50% of oocytes remained at the leptotene stage and no oocytes reached the pachytene stage in E16.5 *Tet1*$^{Gt/Gt}$ ovaries (Fig. 2a). Although pachytene-stage oocytes were observed in E17.5 and E18.5 *Tet1*$^{Gt/Gt}$ ovaries, their percentage is significantly reduced throughout the developmental stages analysed, indicating a developmental block rather than a developmental delay. This notion is also supported by the fact that Tet1 depletion does not affect the percentage of diplotene-stage oocytes at E18.5 (Fig. 2a), and there was no significant difference in body size between *Tet1*$^{+/Gt}$ and *Tet1*$^{Gt/Gt}$ embryos at E16.5 or E18.5 (Supplementary Fig. 6). The significant decrease of pachytene-stage oocytes in *Tet1*$^{Gt/Gt}$ ovaries suggests that Tet1 deficiency may cause aberrant synapsis formation. Considering the increased apoptosis in the E16.5–18.5 *Tet1*$^{Gt/Gt}$ ovaries (Supplementary Fig. 5b, c), severely affected germ cells might be eliminated, explaining the marked reduction in germ-cell numbers in E18.5 *Tet1*$^{Gt/Gt}$ ovaries (Fig. 1d). Thus, meiotic defects are probably the cause of germ-cell reduction in *Tet1*$^{Gt/Gt}$ ovaries.

In normal meiosis, the axial element of the synaptonemal complex starts to form at the leptotene stage, axial-element alignment and synapsis formation are initiated at the zygotene stage and completed

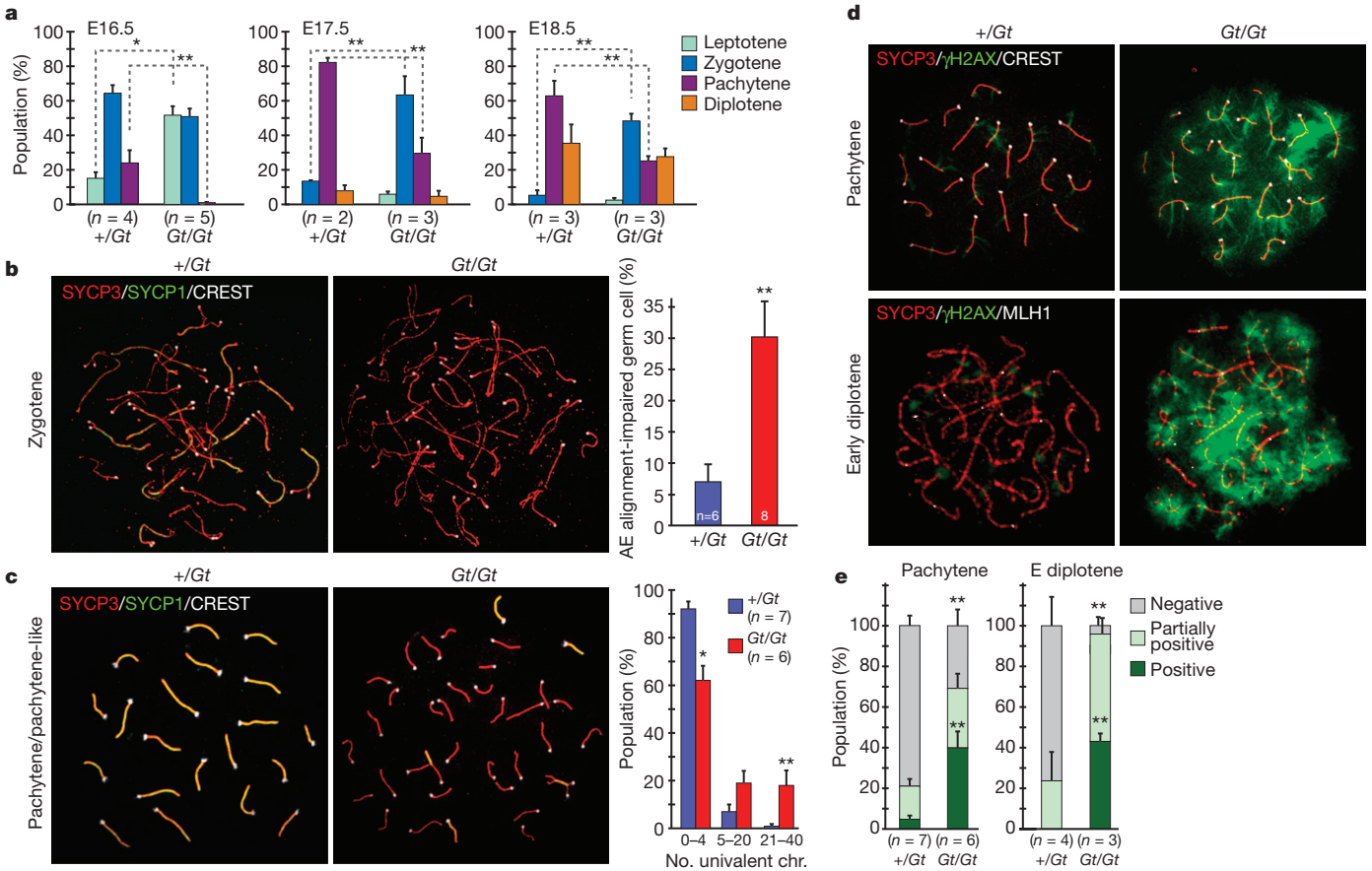

Figure 2 | Meiotic defects in *Tet1*$^{Gt/Gt}$ oocytes. **a**, Distribution of E16.5, E17.5 and E18.5 oocytes in the four sub-stages of meiotic prophase. $n = 2$–5. $^{*}P < 0.05$; $^{**}P < 0.01$ (compared between *+/Gt* and *Gt/Gt*). **b**, Left, representative images of zygotene oocytes co-stained with SYCP3, SYCP1 and CREST antibodies. Right, the percentage of oocytes with impaired axial-element alignment at the zygotene stage. Oocytes that contain less than five SYCP1 foci are counted as axial element (AE)-alignment impaired. $n = 6$–8. $^{**}P < 0.01$. **c**, Left, representative images of pachytene-stage oocytes co-stained with SYCP3, SYCP1 and CREST antibodies. Right, the distribution of oocyte types categorized by the numbers of univalent chromosomes in each pachytene-stage oocyte. $n = 6$–7. $^{*}P < 0.05$; $^{**}P < 0.01$. **d**, Representative images of oocytes co-stained with antibodies against γH2AX, SYCP3 and CREST (pachytene stage), or against γH2AX, SYCP3 and MLH1 (early diplotene stage). **e**, Distribution of oocyte types categorized by the staining pattern of γH2AX in each pachytene- and early diplotene-stage oocyte. Representative images for each group are shown in Supplementary Fig. 9. $n = 3$–7. $^{**}P < 0.01$ (compared with control). All error bars indicate s.e.m.

at the pachytene stage (Supplementary Fig. 7). However, loss of function of Tet1 resulted in an increase in the unpaired synaptonemal complex at zygotene-stage oocytes (Fig. 2b and Supplementary Fig. 7). Despite the presence of SYCP3-positive axial elements, about 30% of the zygonema contained less than four SYCP1-positive transverse filaments in *Tet1*$^{Gt/Gt}$ oocytes (Fig. 2b), suggesting a synapsis-formation defect. Defects in synapsis formation were also observed in the pachytene-stage *Tet1*$^{Gt/Gt}$ oocytes. In these oocytes, the vast majority of axial elements failed to align and instead remained separated from each other as univalent chromosomes (Fig. 2c and Supplementary Fig. 7). Continuous SYCP3 in short stretches of the synaptonemal complex indicates that the oocytes were at a stage corresponding to pachytene. Quantification of pachytene-stage oocytes showed that 92% of the wild-type oocytes had 0–4 univalent chromosomes, but that number dropped to 62% in the *Tet1*$^{Gt/Gt}$ oocytes, which accompanies the increase of the oocytes with five or more univalent chromosomes (Fig. 2c). These results indicate that the Tet1 loss-of-function mutation impaired synapsis formation.

Because about 62% of pachytene-stage oocytes are successful for axial-element pairing, we asked whether they exhibited other defects. At the early phase of meiosis, DNA double-strand breaks (DSBs) are introduced in the initiation of homologous recombination, which can be detected by the presence of γH2AX[1]. As expected, immunostaining revealed the presence of γH2AX throughout the nucleoplasm from the leptotene to zygotene stages in both wild-type and *Tet1*$^{Gt/Gt}$ oocytes (Supplementary Fig. 8). However, although γH2AX is gradually decreased around the pachytene stage and only a few foci remained associated with fully synapsed chromosome cores in wild-type oocytes, cloud-like nuclear staining of γH2AX remained in the *Tet1*$^{Gt/Gt}$ pachytene-stage and even early diplotene-stage oocytes marked by the crossover-specific marker MLH1 (ref. 13; Fig. 2d and Supplementary Fig. 8). Analysis of the γH2AX staining pattern and quantification of the three categories (negative, partially positive and positive) (Supplementary Fig. 9) clearly demonstrated that Tet1 depletion caused accumulation of γH2AX in pachytene- and early diplotene-stage oocytes (Fig. 2e).

The presence of γH2AX in late-stage meiotic oocytes was also confirmed by co-staining of γH2AX with the late-stage meiosis marker MSY2 in E18.5 ovaries (Supplementary Fig. 10). Importantly, a marked increase in γH2AX and cleaved caspase3 double-positive cells was also observed (Supplementary Fig. 10b, c), suggesting that increased apoptotic cell death is probably caused by meiotic defects. Consistent with a DSB repair defect, the DSB repair-associated recombinase RAD51 (ref. 1) remains in pachytene and diplotene oocytes (Supplementary Fig. 11). The presence of γH2AX and delayed removal of RAD51 in the chromosomes indicate that homologous recombination is impaired in *Tet1*$^{Gt/Gt}$ oocytes. Staining with the crossover marker MLH1 indicated that the MLH1 foci numbers are significantly reduced in *Tet1*$^{Gt/Gt}$ pachytene- and early diplotene-stage oocytes (Supplementary Fig. 12), further supporting a homologous recombination defect. Collectively, the above results support the notion that the Tet1 loss-of-function mutation leads to meiotic defects that include univalent chromosome formation, as well as DSB repair and homologous recombination defects.

Previous studies have shown that the establishment of proper pericentric heterochromatin (PCH) structure has an important role in meiosis[14]. Interestingly, immunostaining revealed specific enrichment of 5hmC at PCH of many prophase meiotic chromosomes, and this enrichment is eliminated in *Tet1*$^{Gt/Gt}$ oocytes (Supplementary Fig. 13). As prophase meiotic PCH possesses specific histone modification patterns[15], we asked whether the loss-of-function Tet1 mutation can affect PCH structure by affecting the PCH histone modification pattern. Immunostaining showed that the Tet1 loss-of-function mutation did not affect the PCH histone modification pattern (Supplementary Fig. 14), centromere clustering or localization of heterochromatin protein 1γ (HP1γ) (Supplementary Figs 14 and 15). Collectively, these results suggest that the observed meiotic defect is unlikely to be due to a defect in PCH.

The stage- and cell-type-specific Tet1 expression pattern (Supplementary Fig. 1) and the dual roles of Tet1 in transcription[16,17] suggest that the meiotic defects in *Tet1*$^{Gt/Gt}$ germ cells might be due to aberrant transcription in PGCs. Thus, we purified PGCs from female E13.5 embryos and profiled their transcriptome by messenger RNA sequencing. We choose to focus on this time point because this is when female PGCs enter meiotic prophase after epigenetic reprogramming. We used a recently developed Smart-Seq method[18] and generated more than 20 million unique reads per sample, which allowed us to identify more than 13,000 expressed transcripts in each genotype (Supplementary Table 2). Hierarchical clustering and global correlation analysis indicated that the samples were clearly separated by their genotypes, with Spearman correlation coefficients of 0.98 or 0.99 within biological replicates (Supplementary Fig. 16). Depletion of Tet1 resulted in differential expression of 1,010 genes (false discovery rate (FDR) < 0.05), among which more than 80% (899 genes) were downregulated (Fig. 3a and Supplementary Table 3). Gene Ontology (GO) analysis showed that the most significantly enriched pathways of these downregulated genes are related to the cell cycle ($P < 9 \times 10^{-11}$) and meiosis-related processes ($P < 2 \times 10^{-6}$) (Fig. 3b and Supplementary Fig. 17a). By contrast, no significant enrichment of pathways or biological processes was identified in the upregulated gene group. Importantly, genes known to be crucial for meiosis are downregulated in *Tet1*$^{Gt/Gt}$ PGCs (Fig. 3a and Supplementary Table 3). These genes include *Stra8*, *Prdm9*, *Sycp1*, *Mael* and *Sycp3* (refs 1 and 19–22). Notably, this set of meiotic genes remained downregulated even at

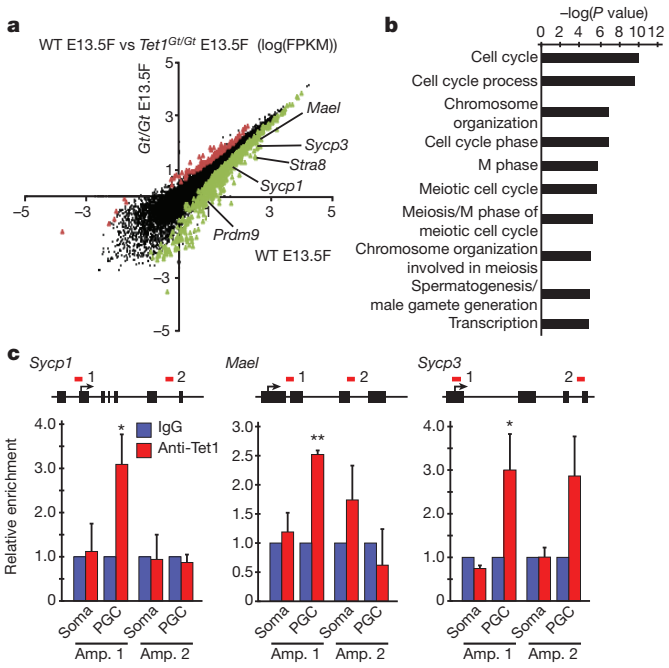

Figure 3 | Tet1 activates meiotic genes through DNA demethylation. **a**, Scatter plot comparing transcriptome of wild-type and *Tet1*$^{Gt/Gt}$ E13.5 female (E13.5F) PGCs. There are 111 and 899 genes that are respectively up- or downregulated (FDR < 0.05). Examples of downregulated meiotic genes include *Mael*, *Sycp3*, *Stra8*, *Sycp1* and *Prdm9*. FPKM, fragments per kilobase of exon per million mapped fragments. **b**, Gene Ontology analysis of downregulated genes in *Tet1*$^{Gt/Gt}$ PGCs with a cut-off FDR < 0.05. The most enriched biological processes based on their *P* values are shown. **c**, ChIP–qPCR analysis of E13.5 wild-type female PGCs using an anti-Tet1 antibody demonstrates binding of Tet1 to the *Sycp1*, *Mael* and *Sycp3* promoters. Top, diagrams of *Sycp1*, *Mael* and *Sycp3* genes, with the analysed regions indicated by red lines. Bottom, relative enrichment of Tet1 compared with IgG control. Amp., amplicon. $n = 3$. Error bars indicate s.e.m. $^*P < 0.05$; $^{**}P < 0.01$.

later developmental stages (Supplementary Fig. 17b, c), consistent with the meiotic defects observed in E16.5 *Tet1*$^{Gt/Gt}$ PGCs. The effects of Tet1 on the expression of at least a subset of these genes are direct, as chromatin immunoprecipitation (ChIP) analysis demonstrated that Tet1 occupies the *Sycp1*, *Mael* and *Sycp3* gene promoters (Fig. 3c). Thus, Tet1 loss directly contributes to aberrant regulation of at least a subset of meiotic genes in PGCs.

To investigate how Tet1 might be involved in activation of these meiotic genes, we performed whole-genome bisulphite sequencing (WGBS) analysis using an ultra-low input, Tn5mC-seq method[23]. We generated 945 million and 302 million reads for *Tet1*$^{Gt/Gt}$ and wild-type PGCs, respectively. After removing clonal reads due to limited input cells, we obtained 14–16 million CpG sites per genotype at 1.76–2.66× genome coverage (Supplementary Table 4), which is more than 100-fold higher than a previous effort[24]. To our knowledge, this provides the most comprehensive methylation map in PGCs so far. Consistent with previous findings[24], we found that PGCs are globally hypomethylated (Fig. 4a), which is verified by immunostaining (Supplementary Fig. 18). Despite no marked increase in global DNA methylation, the DNA methylation level is generally higher in mutant PGCs, particularly in exons, introns, long terminal repeats and intracisternal A particles (Fig. 4a, $P < 0.01$). With the caveat that 2× genome coverage may not allow robust identification of differentially methylated regions (DMRs) between *Tet1*$^{Gt/Gt}$ and wild-type PGCs, we nevertheless performed detailed analysis and identified 4,337 putative DMRs (Supplementary Table 5 and Supplementary Fig. 19) that are mostly located far away from transcriptional start sites (Supplementary Fig. 20a). These putative DMRs are associated with 5,242 genes, among which 255 exhibited altered expression (Fig. 4b and Supplementary Table 6) and are enriched for cell cycle regulation as well as for reproductive and infertility processes (FDR = 0.02) (Supplementary Fig. 20b, c). Furthermore, these DMRs are enriched for Tet1 binding in mouse ES cells[17] ($P < 1 \times 10^{-100}$). To evaluate whether Tet1 binding affects DNA methylation in PGCs, we performed bisulphite sequencing on the three verified Tet1 target genes (Fig. 4c). Consistent with the involvement of Tet1 in DNA demethylation, the methylation levels of the *Sycp1*, *Mael* and *Sycp3* promoters are increased in the *Tet1*$^{Gt/Gt}$ PGCs compared with that in the wild-type PGCs (Fig. 4c). These data indicate that Tet1-mediated demethylation of these genes is probably involved in their activation during PGC development. We note that some downregulated genes, such as *Stra8*, showed no obvious change in DNA methylation indicating that they are either regulated indirectly by Tet1 or regulated in a DNA-methylation-independent manner.

Taken together, our study provides the first evidence that Tet1 is not responsible for global demethylation in PGCs; instead, it has a specific role in meiotic gene activation at least partly through DNA demethylation. Depletion of Tet1 leads to downregulation of meiotic genes, which causes defective meiotic prophase including accumulation of non-repaired DSBs, and formation of univalent chromosomes. The meiotic defects cause loss of oocytes and consequent decrease in fertility and small litter size. Previous studies have established that the DNA methylation levels of certain meiotic genes are decreased concomitant with genomic reprogramming[25]. Our study has extended this observation by demonstrating that Tet1 mediates locus-specific demethylation and subsequent activation of a subset of meiotic genes, revealing a specific function of Tet1 in germ-cell development.

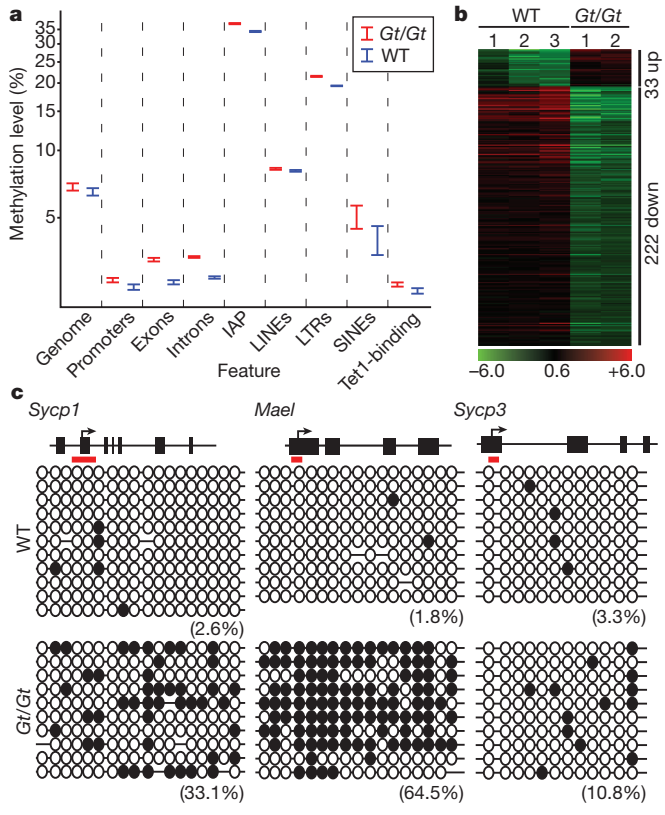

Figure 4 | WGBS analysis of the effect of *Tet1* knockout on DNA methylation in PGCs. **a**, Wild-type E13.5 female PGCs are globally hypomethylated, and depletion of Tet1 only slightly increased the global DNA methylation level. Shown are the DNA methylation levels in the entire mouse genome as well as the various genomic regions. In the last column, the DNA methylation levels at the Tet1-bound regions identified in mouse ES cells[17] were compared. **b**, Heat map of the 255 differentially expressed and DMR-associated genes. **c**, Bisulphite sequencing analysis of the *Sycp1*, *Mael* and *Sycp3* gene promoters of the Tet1-binding site in wild-type and *Tet1*$^{Gt/Gt}$ PGCs. Each CpG is represented by a circle. Open or filled circles represent unmethylated or methylated, respectively. The percentages of DNA methylation are indicated.

METHODS SUMMARY

Mice and characterization of gene-trap allele. A mouse ES cell line containing *Tet1* gene-trap (Gt) allele (RRG140) was purchased from BayGenomics. To generate mice, *Tet1*^{Gt} ES cells were injected into C57BL/6J blastocysts. Heterozygous animals were backcrossed to C57BL/6J strain. Sixty micrograms of cell lysates from control and *Tet1*$^{Gt/Gt}$ ES cells was used for western blot analysis with a Tet1 or β-galactosidase antibody. Dot-blot and mass spectrometry analyses were performed as described[8,9].

RNA isolation, qPCR and RNA-seq analysis using purified PGCs. To purify PGCs, the genital ridges of *Tg(Pou5f1-EGFP)* mice were dissociated with trypsin and hyaluronidase through pipetting before FACS sorting. For expression analysis, complementary DNA was synthesized by Superscript III First-Strand synthesis (Invitrogen) with random primer sets. Quantitative PCR (qPCR) reactions were performed with gene-specific primer sets (Supplementary Table 7). Relative expression levels were determined using comparative C_t values after normalizing with *Gapdh*. For RNA-seq, total RNA was purified from 500–2,000 sorted PGCs using the ZR RNA microprep kit (Zymo Research). The cDNA synthesis and amplification was performed with the SMARTer ultra low input RNA kit (Clontech). Amplified cDNAs (2–70 ng) were then fragmented by Covaris S2 sonicator and converted to sequencing libraries following the Illumina protocol for low input DNA. Bar-coded libraries were pooled and sequenced in three lanes of the Illumina Hiseq 2000 instrument.

ChIP assays and WGBS. ChIP assays were performed using the micro-ChIP method[26]. WGBS analysis was performed using Tn5mC-seq[23]. Conventional bisulphite sequencing was performed using either the EZ DNA methylation Gold kit (Zymo Research) or the EpiTect bisulphite kit (Qiagen). Primers for bisulphite sequencing are listed in Supplementary Table 7.

Full Methods and any associated references are available in the online version of the paper.

Received 14 April; accepted 25 October 2012.
Published online 14 November 2012.

1. Handel, M. A. & Schimenti, J. C. Genetics of mammalian meiosis: regulation, dynamics and impact on fertility. *Nature Rev. Genet.* **11,** 124–136 (2010).
2. Hayashi, K. & Surani, M. A. Resetting the epigenome beyond pluripotency in the germline. *Cell Stem Cell* **4,** 493–498 (2009).

3. Sasaki, H. & Matsui, Y. Epigenetic events in mammalian germ-cell development: reprogramming and beyond. *Nature Rev. Genet.* **9,** 129–140 (2008).
4. Hajkova, P. *et al.* Epigenetic reprogramming in mouse primordial germ cells. *Mech. Dev.* **117,** 15–23 (2002).
5. Seki, Y. *et al.* Extensive and orderly reprogramming of genome-wide chromatin modifications associated with specification and early development of germ cells in mice. *Dev. Biol.* **278,** 440–458 (2005).
6. Kota, S. K. & Feil, R. Epigenetic transitions in germ cell development and meiosis. *Dev. Cell* **19,** 675–686 (2010).
7. He, Y. F. *et al.* Tet-mediated formation of 5-carboxylcytosine and its excision by TDG in mammalian DNA. *Science* **333,** 1303–1307 (2011).
8. Ito, S. *et al.* Role of Tet proteins in 5mC to 5hmC conversion, ES-cell self-renewal and inner cell mass specification. *Nature* **466,** 1129–1133 (2010).
9. Ito, S. *et al.* Tet proteins can convert 5-methylcytosine to 5-formylcytosine and 5-carboxylcytosine. *Science* **333,** 1300–1303 (2011).
10. Tahiliani, M. *et al.* Conversion of 5-methylcytosine to 5-hydroxymethylcytosine in mammalian DNA by MLL partner TET1. *Science* **324,** 930–935 (2009).
11. Dawlaty, M. M. *et al.* Tet1 is dispensable for maintaining pluripotency and its loss is compatible with embryonic and postnatal development. *Cell Stem Cell* **9,** 166–175 (2011).
12. Roeder, G. S. & Bailis, J. M. The pachytene checkpoint. *Trends Genet.* **16,** 395–403 (2000).
13. Edelmann, W. *et al.* Meiotic pachytene arrest in MLH1-deficient mice. *Cell* **85,** 1125–1134 (1996).
14. Takada, Y. *et al.* HP1γ links histone methylation marks to meiotic synapsis in mice. *Development* **138,** 4207–4217 (2011).
15. Tachibana, M., Nozaki, M., Takeda, N. & Shinkai, Y. Functional dynamics of H3K9 methylation during meiotic prophase progression. *EMBO J.* **26,** 3346–3359 (2007).
16. Williams, K. *et al.* TET1 and hydroxymethylcytosine in transcription and DNA methylation fidelity. *Nature* **473,** 343–348 (2011).
17. Wu, H. *et al.* Dual functions of Tet1 in transcriptional regulation in mouse embryonic stem cells. *Nature* **473,** 389–393 (2011).
18. Ramskold, D. *et al.* Full-length mRNA-Seq from single-cell levels of RNA and individual circulating tumor cells. *Nature Biotechnol.* **30,** 777–782 (2012).
19. de Vries, F. A. T. *et al.* Mouse Sycp1 functions in synaptonemal complex assembly, meiotic recombination, and XY body formation. *Genes Dev.* **19,** 1376–1389 (2005).
20. Hayashi, K., Yoshida, K. & Matsui, Y. A histone H3 methyltransferase controls epigenetic events required for meiotic prophase. *Nature* **438,** 374–378 (2005).
21. Soper, S. F. *et al.* Mouse maelstrom, a component of nuage, is essential for spermatogenesis and transposon repression in meiosis. *Dev. Cell* **15,** 285–297 (2008).
22. Wang, H. & Höög, C. Structural damage to meiotic chromosomes impairs DNA recombination and checkpoint control in mammalian oocytes. *J. Cell Biol.* **173,** 485–495 (2006).
23. Adey, A. & Shendure, J. Ultra-low-input, tagmentation-based whole-genome bisulfite sequencing. *Genome Res.* **22,** 1139–1143 (2012).
24. Popp, C. *et al.* Genome-wide erasure of DNA methylation in mouse primordial germ cells is affected by AID deficiency. *Nature* **463,** 1101–1105 (2010).
25. Maatouk, D. M. *et al.* DNA methylation is a primary mechanism for silencing postmigratory primordial germ cell genes in both germ cell and somatic cell lineages. *Development* **133,** 3411–3418 (2006).
26. Dahl, J. A. & Collas, P. A rapid micro chromatin immunoprecipitation assay (microChIP). *Nature Protocols* **3,** 1032–1045 (2008).

Supplementary Information is available in the online version of the paper.

Acknowledgements We thank J. Wang and W. Jiang for FACS sorting, A. Adey and J. Shendure for sharing reagents and protocols for Tn5mC-seq, and H.-L. Fung for Illumina sequencing. This work was partially supported by U01DK089565 (National Institutes of Health) (to Y.Z.), R01GM097253 and CIRM BRB3-05083 (to K.Z.). Y.Z. is an Investigator of the Howard Hughes Medical Institute. D.D. is a CIRM-UCSD pre-doctoral fellow.

Author Contributions Y.Z. conceived the project; S.Y., K.H. and Y.Z. designed the experiments; S.Y., K.H., R.L., L.S. and A.I. performed the experiments; S.Y., K.H., R.L., D.D., K.Z. and Y.Z. analysed and interpreted the data; S.Y., K.H., R.L., K.Z. and Y.Z. wrote the manuscript.

Author Information RNA-seq and WGBS data have been deposited in the Gene Expression Omnibus under accession numbers GSE41908 and GSE41912, respectively. Reprints and permissions information is available at www.nature.com/reprints. The authors declare no competing financial interests. Readers are welcome to comment on the online version of the paper. Correspondence and requests for materials should be addressed to K.Z. (kzhang@bioeng.ucsd.edu) or Y.Z. (yzhang@genetics.med.harvard.edu).

METHODS

Mice and characterization of gene-trap allele. All animal studies were performed in accordance with guidelines of the Institutional Animal Care and Use Committee at the University of North Carolina at Chapel Hill. A mouse ES cell line containing the *Tet1* gene-trap (Gt) allele (RRG140) was purchased from BayGenomics. The insertion site for the gene-trap cassette was identified by Southern blotting, genomic sequencing and allele-specific PCR. Primers used for genotyping are listed in Supplementary Table 7. To generate mice, $Tet1^{Gt}$ ES cells were injected into C57BL/6J blastocysts. Germ-line transmission was confirmed by PCR genotyping with allele-specific primers (Supplementary Table 7). Heterozygous animals were backcrossed to the C57BL/6J strain. Most experiments were performed using mice after backcrossing for at least six generations.

ES-cell derivation, western blot, dot-blot and mass spectrometry analysis. The $Tet1^{Gt/Gt}$ ES cell line was derived as described previously[27] with some modifications. In brief, E3.5 blastocysts were isolated from mating of heterozygous males and females. Each blastocyst was plated on a 96-well plate with feeder layer (mitomycin C-inactivated mouse embryonic fibroblasts), and cultured with conventional ES medium (DMEM/F12 (Gibco) supplemented with 15% FBS and 1,000 U ml^{-1} ESGRO (Millipore)). After overnight incubation, medium was changed to two inhibitors plus LIF (2iL) medium (N2B27 medium supplemented with 20% KSR (Invitrogen), 3 μM CHIR99021 (Stemgent), 15 μM PD0325901 (Stemgent) and 1,000 U ml^{-1} ESGRO). After 5–6 days of culture, ES cells were subcloned with 0.05% Trypsin/EDTA (Gibco) and seeded onto new feeder layer. In general, ES cells are established after 5–7 passages. Genotype was determined by genomic PCR after establishment of ES lines. For western blotting analysis, feeder cells were removed and ES cells were collected after 1 day culture on the Matrigel (BD)-coated plates. Sixty micrograms of cell lysates from control and $Tet1^{Gt/Gt}$ ES cells was used for western blot analysis with a Tet1 or β-galactosidase antibody. Dot-blot and mass spectrometry analyses were performed as previously described[8,9].

RNA isolation and qRT–PCR from purified PGCs and somatic cells. The transgenic mouse line containing the GOF18ΔPE-EGFP (*Tg(Pou5f1-EGFP)*) gene was purchased from Jackson Laboratory. Genital ridge cells were dissociated with 0.05% trypsin/EDTA treatment with pipetting. After washing with phosphate buffer medium (PB1)/BSA solution, tissues were incubated in hyaluronidase and then passed through a cell strainer. Germ cells and somatic cells were purified based on the expression of green fluorescent protein (GFP) using FACS Aria II flow cytometry (BD Bioscience). Total RNA was isolated using the RNeasy mini kit (Qiagen), and cDNA was generated with random primer sets and Superscript III first-strand synthesis system (Invitrogen). Real-time qPCR reactions were performed on an ABI ViiA7 sequence detection system (Applied Biosystems) using SYBR Green (Applied Biosystems). Relative gene expression levels were analysed using comparative C_t methods, in which C_t is the cycle threshold number, and normalized to *Gapdh*. qRT–PCR primers are listed in Supplementary Table 7.

Immunocytological analysis of spreads. To prepare the spreads, dissected E11.5 genital ridges were dissociated by 0.05% trypsin/EDTA. After centrifugation, cells were suspended in PBS and dropped onto slide glasses dipped into fixative (1% paraformaldehyde, 0.15% Triton X-100 and 3 mM dithiothreitol, pH 9.2). The slide glasses were kept overnight in a humidified box at 4 °C. The slides were washed in water containing 0.4% Photoflow (Kodak), and completely dried at room temperature. Surface spreads of ovary cell suspension were prepared as described[28] with some modifications. In brief, the ovary was minced with two forceps and dissociated by pipetting in PBS. An equal volume of hypotonic buffer (30 mM Tris-HCl, pH 8.3, 5 mM EDTA, 1.7% sucrose and 0.5% trisodium citrate dihydrate) was added to the cell suspension. After 7 min of incubation, cells were centrifuged for 5 min and resuspended in 100 mM sucrose. The cell suspension was spread onto glass slides dipped into fixative with the same method as PGC spreads.

To stain spreads, dried slide glasses were washed with 0.1% Triton X-100/PBS (PBST) for 10 min, and incubated with blocking buffer (3% BSA, 2% donkey serum/PBST) for 1 h at room temperature. For the staining with anti-5mC and -5hmC antibodies, spreads were treated with HCl solution for 20 min at room temperature, followed by washes in PBST. Spreads were then incubated with blocking buffer and primary antibodies. Spreads were incubated with primary antibody at 4 °C overnight, followed by washes with PBST, and incubation with appropriate secondary antibodies for 1 h at room temperature.

H&E and immunostaining analysis. Paraffin-embedded ovary and testis samples collected from 8-week-old mice were cut to 7-μm thickness and stained with H&E. For counting, serial sections were stained with H&E, and the oocyte numbers were manually counted at 100-μm intervals throughout the entire ovary. For immunofluorescence staining, tissues fixed with 4% paraformaldehyde/PBS overnight at 4 °C were embedded in OCT compound (Sakura) and cut to 10-μm thickness. After washing with PBS, sections were permeabilized with 0.4% Triton X-100/PBS for 20 min at room temperature, followed by 1-h incubation with blocking buffer (3% BSA, 2% donkey serum/PBST) at room temperature. Then, sections were incubated at 4 °C with primary antibody overnight, followed by PBST washes and incubation with appropriate secondary antibodies at room temperature for 1 h. When sections were stained with anti-5hmC, sections were treated with HCl solution (4 N HCl, 0.1% Triton-X 100 in distilled water) for 20 min at room temperature, followed by washing, and incubation with blocking buffer and primary antibodies. To count the oocyte number, one in five consecutive sections was taken at regular interval throughout the entire gonad, stained with germ-cell marker and analysed by ImageJ software.

Antibodies. The antibodies used in this study include anti-SYCP3 (rabbit, Abcam ab15093), anti-SYCP3 (mouse, Abcam ab97672), anti-SYCP3 (goat, Santa Cruz sc-20845), anti-γH2AX (mouse, Millipore 05-636), anti-γH2AX (rabbit, Cell Signaling 2577), anti-CREST (human, Antibodies 15-235), anti-RAD51 (rabbit, Calbiochem PC130), anti-RAD51 (mouse, Abcam sb88572), anti-MLH1 (mouse, BD Pharmingen 550838), anti-SYCP1 (rabbit, Abcam ab15090), anti-5hmC (Active Motif 39769), anti-Tet1 (for western blotting, see ref. 8; for immunostaining, Millipore 09-872), anti-cleaved caspase3 (rabbit, Cell Signaling 9661), anti-SSEA1 (mouse, Millipore MAB4301), anti-MVH (rabbit, Abcam ab13840), anti-TRA98 (rat, BioAcademia 73-003), anti-MSY2 (goat, Santa Cruz sc-21314), anti-histone H3K9me2 (mouse, Millipore 05-1249), anti-histone H3K9me3 (rabbit, Abcam ab8898), anti-histone H4K20me3 (mouse, Abcam ab78517) and anti-HP1γ (goat, Abnova PAB6885).

Staging of meiotic germ-cell prophase. Staging of oocytes was performed based on the appearance of axial elements (SYCP3 staining) and centromere numbers (CREST staining)[29]. In brief, in wild-type the leptotene stage is defined by the appearance of dot-like SYCP3 signals and clustering of centromeres into several loci in the nucleus; the zygotene stage is defined as the start of synapsis, and fibre-like SYCP3 staining and pairing of 30–80% of centromeres are observed; in the pachytene stage all axial elements are paired and 20 foci of CREST are visible at the end of the SYCP3 stretch; the diplotene stage is defined by more than 20 CREST signals, coincident with desynapsis, and fragmentation of SYCP3 is also observed. Because female germ cells enter meiosis in a synchronous manner, leptotene- and zygotene-stage germ cells can be obtained from E16.5 ovary, whereas pachytene and diplotene germ cells are obtained from the E18.5 ovary in the wild type. In $Tet1^{Gt/Gt}$ ovaries, leptotene-stage germ cells were obtained from the E16.5 ovary, whereas zygotene, pachytene and diplotene germ cells were obtained from E18.5 ovaries. Pachytene-like stage oocytes in the $Tet1^{Gt/Gt}$ ovary were defined as those that contain condensed and short axial element without any nick, no clear clustering of centromeres, and more than 20 SYCP3 stretches.

RNA-seq and GO analysis. Total RNA was purified from 500–2,000 sorted PGCs using the ZR RNA microprep kit (Zymo Research). The cDNA synthesis and amplification was performed with the SMARTer ultra low input RNA kit (Clontech). The amplified cDNA (2–70 ng) was then fragmented by Covaris S2 sonicator (Covaris) and converted to sequencing libraries following the Illumina construction protocol for low input DNA (Illumina). Bar-coded libraries were pooled and sequenced in three lanes of the Illumina Hiseq 2000 instrument.

mRNA-seq reads generated from each sample were aligned to the mouse genome (mm9, NCBI build 37) with Bowtie/Tophat v1.3.1 (http://tophat.cbcb.umd.edu), which allows mapping across splice sites by reads segmentation. All programs were used with default setting unless otherwise specified. Mapped reads (83–84% of total reads) were subsequently assembled into transcripts guided by reference annotation (mm9, USCS gene annotation) with Cufflinks v1.0.3 (http://cufflinks.cbcb.umd.edu). The expression level of each transcript was quantified with normalized FPKM. Two or three biological replicates were used in each genotype to identify transcripts that showed significant differences at a cut-off FDR < 0.05 between wild type and $Tet1^{Gt/Gt}$ by Cuffdiff v1.0.3. Functional annotation of significantly different transcripts and enrichment analysis was performed with DAVID (http://david.abcc.ncifcrf.gov).

ChIP assays and bisulphite sequencing. ChIP assays were performed using the micro-ChIP method[26]. In brief, GFP-positive and -negative cells from E13.5 genital ridges were cross-linked with a final concentration of 1% formaldehyde soon after sorting. After incubation at room temperature for 8 min, the reaction was stopped by the addition of 125 mM glycine. Sonicated chromatins were subjected to incubation with anti-Tet1-coated Dynabeads Protein A complex at 4 °C for 2 h. After extensive washing, immunoprecipitated DNA was eluted from the beads, and analysed on an ABI ViiA7 sequence detection system (Applied Biosystems) using SYBR Green (Invitrogen). Primers for the ChIP assay are listed in Supplementary Table 7.

Bisulphite sequencing was performed using a protocol associated with either the EZ DNA methylation Gold kit (Zymo Research) or the EpiTect bisulphite kit (Qiagen). In brief, about 20 ng of sodium bisulphite-treated DNA samples was subjected to PCR amplification using the first set of primers; PCR products were used as templates for a subsequent PCR reaction using nested primers. The PCR products of the second reaction were then subcloned using the Invitrogen TA

cloning kit following the manufacturer's instruction. PCRs and subcloning were performed in duplicate for each sample. The clones were sequenced using the M13 forward primer. Primers for bisulphite sequencing are listed in Supplementary Table 7.

WGBS and data analysis. WGBS analysis was performed using Tn5mC-seq[23]. In brief, genomic DNA was isolated using the Wizard kit (Promega) when >5,000 cells were available, whereas samples with <5,000 cells were directly lysed in a hypotonic lysis buffer (10 mM Tris-HCl, pH 7.5, 10 mM NaCl and 3 mM $MgCl_2$) with 1% NP40 and 0.2 arbitrary units (AU) ml^{-1} protease (Qiagen). Resultant DNA were fragmented and attached with a 5′-methylated adaptor by Tn5-transposon-based tagmentation. A 3′-methylated adaptor was added during gap-filling and ligation. Tagged DNA fragments were bisulphite-converted using the Imprint kit (Sigma) or Lightning kit (Zymo), followed by PCR amplification with Illumina adaptors. Bar-coded libraries were pooled and sequenced with Illumina Hiseq 2000 instrument.

Bisulphite-converted sequencing data were processed using the BisReadMapper analysis pipeline[30]. In brief, reads were aligned to the mouse reference genome (mm9) using SOAP2. Libraries processed with the Sigma Imprint kit contain a mixture of fully converted and poorly converted reads. A post-mapping filtering was performed to remove unconverted reads based on the criterion that cytosine in the non-CpG context is present at <1.2% in the raw sequencing reads, which ensured a bisulphite conversion rate of >98% in the filtered reads, as estimated by the percentage of unmethylated cytosines on the mitochondrial chromosome. Libraries processed with the Zymo lightning kit were fully converted, such that the post-mapping filtering was not necessary. Data from the two batches of libraries were pooled as global analysis on the two batches yielded consistent results. The global methylation distribution plot was generated using the average methylation levels of CpGs in 10-kb non-overlapping bins along the genome. DMRs between genotypes were identified by comparing the fraction of methylated cytosines in a sliding window that contains at least six CpG sites based on chi-square test. Repetitive regions were masked before DMR calling. Adjacent candidate DMRs (<250 base pairs (bp) apart) were joined, and the flanking non-informative CpG sites were further trimmed. We required that there are at least 20 methylated or unmethylated cytosine observations for each sample in a DMR, and the mean methylation difference is at least 0.2. The FDR was empirically estimated to be ~10%, by applying the same procedure on randomly permutated data sets in which the methylation level of each CpG site was randomly assigned to a different CpG site in the genome while maintaining the global distribution of CpG methylation in each sample. Identified DMRs were correlated with Tet1-binding sites defined in ESCs[17] by requiring >1 bp overlapping using BEDtools (http://code.google.com/p/bedtools/). The FDR was then tested by 100 permutations of randomly placed DMRs along the genomes. DMRs were assigned to potential target genes and functional characterized by GREAT (http://great.stanford.edu/public/html/splash.php). For visualization, locally smoothed methylation levels were calculated by the Bsseq package with parameter of ns = 40, h = 2,000 (in which ns is the minimum methylation loci in a smoothing window, and h is the minimum smoothing window size in bases) to obtain high confidence methylation levels for each genotypes (http://www.bioconductor.org/packages/devel/bioc/html/bsseq.html). We did not use Bsseq for DMR calling owing to a high false positive rate on the low-coverage data we have.

27. Markoulaki, S., Meissner, A. & Jaenisch, R. Somatic cell nuclear transfer and derivation of embryonic stem cells in the mouse. *Methods* **45,** 101–114 (2008).
28. Soper, S. F. C. *et al.* Mouse maelstrom, a component of nuage, is essential for spermatogenesis and transposon repression in meiosis. *Dev. Cell* **15,** 285–297 (2008).
29. Kouznetsova, A., Novak, I., Jessberger, R. & Hoog, C. SYCP2 and SYCP3 are required for cohesin core integrity at diplotene but not for centromere cohesion at the first meiotic division. *J. Cell Sci.* **118,** 2271–2278 (2005).
30. Diep, D. *et al.* Library-free methylation sequencing with bisulfite padlock probes. *Nature Methods* **9,** 270–272 (2012).